Electrode contact impedance sensitivity to variations in geometry

2012 Physiol. Meas. 33 817

(http://iopscience.iop.org/0967-3334/33/5/817)

Physiol. Meas. **33** (2012) 817–830 doi:10.1088/0967-3334/33/5/817

Electrode contact impedance sensitivity to variations in geometry

Roberto Cardu[1], **Philip H W Leong**[2], **Craig T Jin**[2] **and Alistair McEwan**[2]

[1] ARCES, University of Bologna, Italy
[2] University of Sydney, Australia

E-mail: rcardu@arces.unibo.it

Received 27 November 2011, accepted for publication 24 January 2012
Published 24 April 2012
Online at stacks.iop.org/PM/33/817

Abstract
Electrode contact impedance is a crucial factor in physiological measurements and can be an accuracy-limiting factor when performing electroencephalography and electrical impedance tomography. In this work, standard flat electrodes and micromachined multipoint spiked electrodes are characterized with a finite-element method electromagnetic solver and the dependence of the contact impedance on geometrical factors is explored. It is found that flat electrodes are sensitive to changes in the outer skin layer properties related to hydration and thickness, while spike electrodes are not. The impedance as a function of the effective contact area, number of spikes and penetration depth has also been studied and characterized.

Keywords: contact impedance, bio-potential recordings, EIT, EEG, spiked electrodes

(Some figures may appear in colour only in the online journal)

1. Introduction

A common issue when recording bio-potentials is related to the impact of the electrode contact impedance. An impedance mismatch between electrodes can diminish the common mode rejection ratio (CMRR) of the system, thus increasing power-line interference sensitivity (Huhta and Webster 1973). In order to increase the CMRR, an additional driven right leg (DRL) loop is usually implemented to mitigate such effect (Winter and Webster 1983). Custom active circuitry can also be implemented to measure the contact impedance and ensure that a sufficient CMRR is achieved (Degen and Jackel 2008, Spinelli *et al* 2006, Guermandi *et al* 2011).

Electroencephalography (EEG) consists in the recording of electrical activity along the scalp, as produced by the firing of neurons within the brain. Localization of EEG signal sources is an established method for providing low-cost and high-temporal resolution brain activity maps (Michel *et al* 2004). Localization accuracy is greatly influenced by unknown brain,

skull and skin conductivities. Conductivity maps can be determined with the use of electrical impedance tomography (EIT), which is usually performed on a body by applying known currents and measuring voltages at its surface (Brown 2003, Holder 2004). The two techniques can also be combined, but bulky hardware and low configurability pose some limitations. Recently Guermandi *et al* (2011) have presented an integrated circuit (IC) integrating the two functions. EIT in fact might give *a priori* information for the EEG source localization problem and possibly provide complementary information since the physical principle observed is correlated but different (Gonçalves *et al* 2000).

In clinical practice, Ag/AgCl electrodes along with a conductive paste or gel are commonly used for bio-potential acquisition. This setup has proven to be effective for many applications, but its use is mostly limited to clinical settings or research labs, due to the difficulties in establishing robust and long-lived electrical contacts. It is often desirable to monitor bio-potential activity for an extended period of time, a practice normally referred to as Holter monitoring. In order to investigate abnormalities that appear over longer time frames, numerous low-power EEG implementations have been presented for portable applications (Wise *et al* 2004, Rabaey 2011). Dry electrodes applied without glue are more convenient for the wearer and are significantly faster to apply in emergencies, but suffer from movement artifacts that are often large enough to cause the amplifier to saturate during acquisition (Searle and Kirkup 2000). The application of electrical currents in EIT and functional stimulation can also be affected by contact impedance as it introduces variability into the injected currents. Contact impedance mismatches as small as 20% (McEwan *et al* 2007) can make an EIT image meaningless (Boone and Holder 1996, Boyle and Adler 2011). Thus, investigating the electrode properties is critical for EIT applications.

In this work, the sensitivity of the electrode contact impedance is investigated as a function of different electrode geometries using a finite-element method (FEM) solver, following the planar electrode modeling presented by Hua *et al* (1993) and Martinsen *et al* (1999). Section 2 introduces the basic electromagnetic (EM) theory behind the contact impedance problem, while sections 3 and 4 illustrate methods and results for different simulation setups, flat electrodes and micromachined multipoint spiked electrodes, as well as the major limitations of a pure EM approach for the investigation of contact impedance. An analytical expression is fitted to the results to provide an easy method of determining the contact impedance of electrodes based on the area, frequency, spike number and spike depth. Conclusions are drawn in section 5.

2. EM theory

EM simulations have been carried out with the FEM tool Comsol Multiphysics® (Comsol 2011). Comsol® can be used to numerically solve partial differential equations. For a nonmagnetic material such as a biological tissue, Maxwell's equations, with the inclusion of the equation of continuity, can be written as

$$\nabla \times \mathbf{H} = \mathbf{J} + \frac{\partial \mathbf{D}}{\partial t}$$

$$\nabla \cdot \mathbf{B} = 0$$

$$\nabla \times \mathbf{E} = -\frac{\partial \mathbf{B}}{\partial t}$$

$$\nabla \cdot \mathbf{D} = \rho(\mathbf{r}, t)$$

$$\nabla \cdot \mathbf{J} = -\frac{\partial \rho(\mathbf{r}, t)}{\partial t},$$

where $\rho(\mathbf{r}, t)$ is the charge density, $\mathbf{J}$ is the current density, $\mathbf{E}$ is the electric field, $\mathbf{D} = \varepsilon\mathbf{E}$ is the electric displacement with ε the electric permittivity, $\mathbf{B}$ is the magnetic field and $\mathbf{H} = \mathbf{B}/\mu$ is the magnetic intensity with μ the magnetic permeability. When studying contact impedance for bio-potential acquisition such as EEG or EIT, we make the following assumptions that greatly simplify the problem:

(1) negligible external $\mathbf{B}$ field.
(2) quasi-static limit $\left(\frac{\partial \mathbf{D}}{\partial t} = 0\right)$.

The first of the two assumptions are justified as long as there is no electromagnetic interference (EMI). This means that the EIT and EEG should be performed in a proper clinical environment and no other EM disturbance such as that might be caused by an imaging technique, e.g. MRI, trans-cranial magnetic stimulation (TMS) or ablation, is performed concurrently. EMI could still be present at the power-line frequency (50 or 60 Hz), which is one of the key issues when recording EEG and EIT. As explained in section 1, an electrode contact impedance mismatch could easily cause a decrease in the system's CMRR. Measurement of the contact impedance can be carried out at frequencies below or above the power-line frequency, therefore allowing us to neglect the $\mathbf{B}$ field. Techniques to mitigate such interference, such as wire twisting (Huhta and Webster 1973) and increasing the CMRR through a DRL loop (Winter and Webster 1983), exist, but are out of the scope of the present work. Additional EMI could occur from mobile phones when measuring the contact impedance, but this is nullified if the devices are held at a proper distance from the patient and EEG/EIT instrumentation (Tri *et al* 2005).

The quasi-static approximation is valid as long as the EIT injected frequency is low enough for the EM propagation delay to be neglected (Weiping Wang and Eisenberg 1994). For a 100 kHz EIT signal in a human head with a radius$\rho_h = 0.2$ m, the propagation delay is approximately given by $\rho h/c$, where c is the speed of the EM waves in the body, which approaches the speed of light. This results in a delay which is less than a nanosecond, much smaller than the signal period of 10^{-4} s.

Secondly, the ratio of the displacement current to the conduction current is of the order of $\omega\varepsilon/\sigma$ (Bowtell and Bowley 2000). For biological tissues, the permittivity ε varies with frequency, ranging between 10^{-7} at 10 kHz and 10^{-5} at 10 Hz (Weiping Wang and Eisenberg 1994), with $\omega\varepsilon/\sigma$ resulting between 10^{-2} and 10^{-3}. This means that we can ignore the contribution of the displacement current. With such assumptions, the electric field can be expressed solely in terms of the electric potential. Combining the time-harmonic equation of continuity and assuming no charge variation in the volume and an applied external current,

$$\nabla \cdot \mathbf{J} = \nabla \cdot (\sigma\mathbf{E} + \mathbf{J}^e) = -\mathrm{j}\omega\rho(\mathbf{r}, t) = 0 \tag{1}$$

with the equation

$$\nabla \cdot \mathbf{D} = \rho(\mathbf{r}, t), \tag{2}$$

one obtains

$$-\nabla \cdot ((\sigma + \mathrm{j}\omega\varepsilon)\nabla V - \mathbf{J}^e) = 0. \tag{3}$$

The external boundary conditions are set as

$$\mathbf{n} \cdot \mathbf{J} = 0 \tag{4}$$

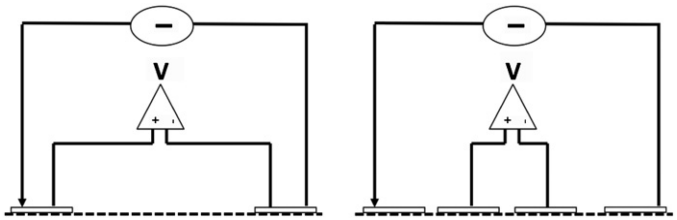

Figure 1. Two-electrode (left) and four-electrode (right) impedance measurements.

at all points other than at the current injecting and absorbing electrodes, which are set respectively as

$$\int \frac{V}{\text{area}} = \mathbf{Z} \cdot \mathbf{I} \tag{5}$$

and

$$V = 0 \tag{6}$$

with the impedance, which is frequency dependent and that is usually represented as a complex number with a real and imaginary part,

$$\mathbf{Z} = \text{Re}\{\mathbf{Z}\} + j\,\text{Im}\{\mathbf{Z}\}, \tag{7}$$

accounting for its resistive and reactive components. On the internal boundaries between two adjacent domains D_1 and D_2, continuity is given by

$$\mathbf{n} \cdot (\mathbf{J}_1 - \mathbf{J}_2) = 0. \tag{8}$$

Equation (3), along with the boundary equations (4)–(6) and (8), constitutes a problem that can be numerically solved with Comsol®.

3. Methods

Contact impedance is evaluated in a real-life scenario with either two or four electrodes as shown in figure 1.

Four-electrode measurements achieve higher accuracy as they allow one to separate the contribution of the contact impedance from the underlying volume. The assumption is that high input-impedance amplifiers drain negligible current and if two separate electrodes are used for voltage sensing, no significant voltage drop should occur on these electrodes. Subtraction between the two measurements yields the contact impedances of the current injecting and absorbing electrodes. This is subject to the approximation that the two current injecting and sensing electrodes cannot be placed in the same location, unless concentric electrodes are used.

Nevertheless, four-electrode measurements are not always a feasible option due to the extra cost of the additional electrodes. In the work presented by Guermandi *et al* (2011), an active electrode for simultaneous EIT and EEG measurements has been introduced, along with continuous contact electrode impedance monitoring between two electrodes. For this reason, a two-electrode simulation environment has been chosen in this paper.

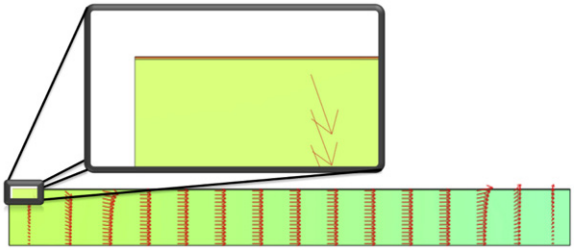

Figure 2. 2D two-electrode simulation.

3.1. Comparison between different simulation setups

In order to validate the simulation, several steps have been taken. First of all, a 2D simulation for flat, square electrodes has been performed. The simulation environment is depicted in figure 2, where the volume depth is set to 1 cm and ideal electrodes (1 cm $\times$ 1 cm) are placed 5 cm apart. The arrows represent the current flow as current is introduced into the left electrode and returned into the right electrode.

As can be seen in figure 2, the skin is characterized as a two-layer volume: a thicker conductive layer of 0.6 cm (deep tissues containing a granular layer) and a thin, resistive layer of 32 μm of stratum corneum (SC), as presented by Yamamoto and Yamamoto (1976, 1986) and Gabriel *et al* (1996). Dead cells mainly form the latter, and because of its low conductivity, are usually removed by abrasion when performing EEG or EIT. This model is in accordance with the literature (Chi *et al* 2010, Gandhi *et al* 2011) for dry electrodes. In such models, a resistor and a capacitor are used in parallel to represent the SC, with an additional series resistor for the underlying skin as its properties are mainly resistive. Additionally, a half-cell potential generator can be considered, but due to its dc nature it can be neglected for our purposes, as EEG and EIT are not performed with direct currents. This and other model limitations are discussed in section 4.4.

The resulting impedance for this configuration is compared with a full 3D simulation, shown in figure 3, a 3D equivalent model to the one presented in figure 2.

In both figures 2 and 3, the color scale represents the electric potential, while the arrows represent the total current density. No constraints on current density uniformity have been imposed. In figure 3, this may seem constant as a function of depth but that is only a visual representation within the FEM solver. As the tissue layer is quite thin (0.6 cm), current density changes are small; hence, they can be hard to distinguish. The injecting electrode is the one with the higher potential (in red), while the absorbing electrode is kept at ground (in blue). The setup of the two previous examples (in 2D or 3D) is the most common scenario for contact impedance measurements, with the assumption that the volume between the two electrodes is rather small compared to the contact impedance at lower frequencies. When performing an EM simulation, the setup can be simplified, including only one standard electrode and a ground electrode underneath the skin, as depicted in figure 4. In this setup, current is injected from the top face and absorbed at the bottom face and the current density is hence oriented along the z-axis. This allows focusing the study on the impact of the SC rather than the underlying volume.

3D FEM simulations require a high number of elements and geometric simplification is the key factor in order to be able to obtain significant simulation data. This is critical for memory usage as the ratio of the overall geometry (10^{-2} m) to the SC thickness (30^{-6} m) is very large, requiring a problematically large number of mesh elements. Although it has been shown that 2D simulations are accurate, electrode geometries such as needles or micromachined

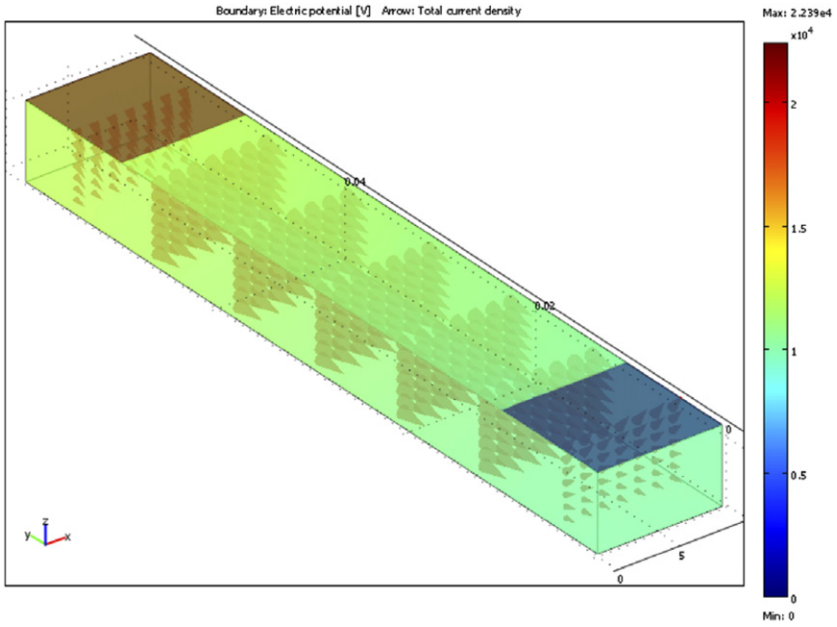

Figure 3. 3D two-electrode simulation.

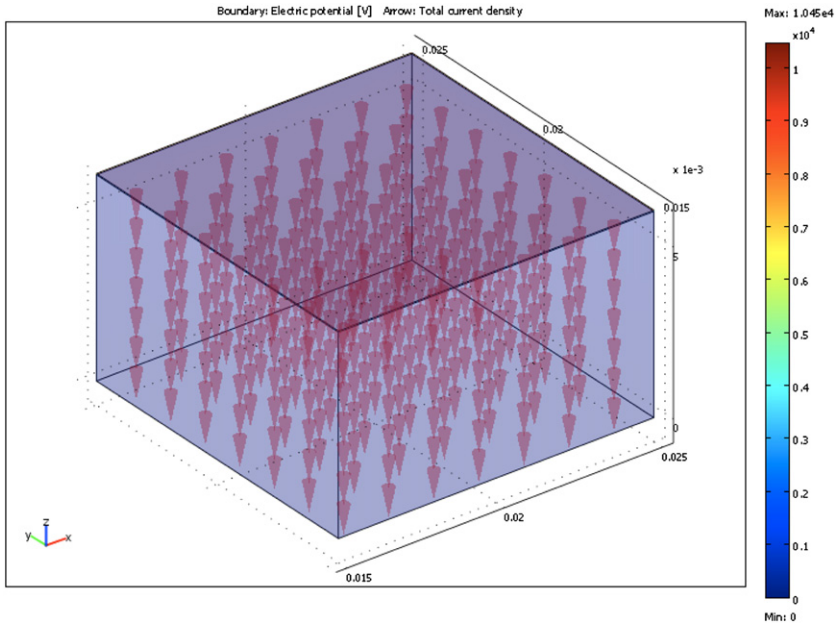

Figure 4. 3D single-electrode setup.

multipoint spiked electrodes cannot be simulated in a 2D environment. The simulation setup in figure 4 represents a reasonable trade-off for a 3D environment. In order to include possible fringing effects, which cannot be simulated in 2D, the volume has been expanded by a factor of 2 in the x and y directions, as shown in figure 5, with the injecting surface on the top face

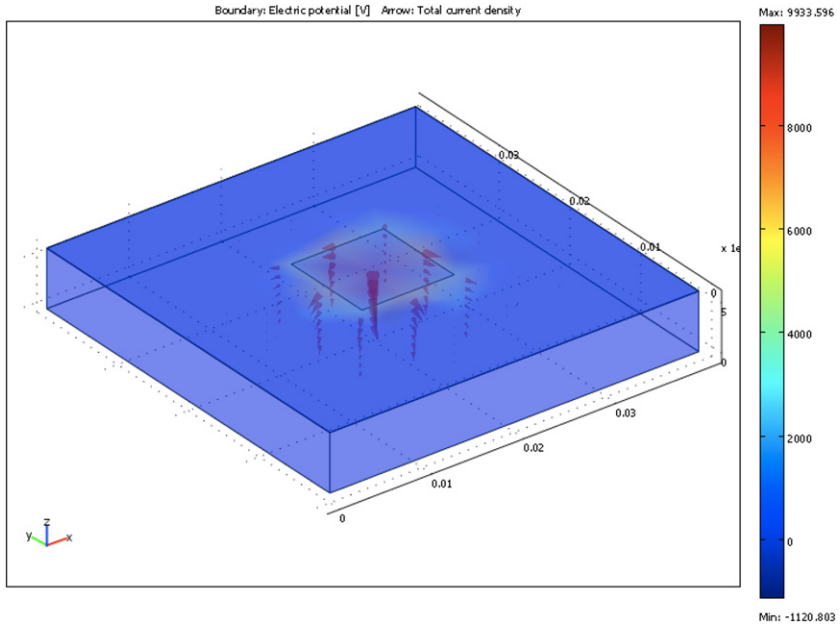

Figure 5. 3D single-electrode expanded geometry to include fringing fields.

kept constant. This choice enables the current to flow unrestricted by tight boundaries, and hence gives a more accurate representation of the physical problem under study. This can be seen as the current density in figure 5 has a component in the x and y directions, as opposed to the strictly vertical current density shown in figure 4.

3.2. Impact of the contact area on flat electrodes

One of the key factors when considering the electrode contact impedance is given by the contact area. In practice, when a metal plate is used, its entire surface is not always in contact with the skin. This is caused by multiple factors, such as skin pores and hair obstructing the electrode–skin interface. In order to simulate such scenarios, parametric simulations as a function of the effective electrode area have been performed.

3.3. Micromachined multipoint spiked electrodes

With the development of MEMS technology, new dry micromachined multipoint spiked electrodes have been presented (Griss *et al* 2002, Gramatica *et al* 2006). Such electrodes offer some benefits when compared to other dry electrodes, and wet Ag/AgCl electrodes. Standard clinical use of wet electrodes for EEG or EIT measurements requires the abrasion of the SC layer. This is a time-consuming practice and can make the patient uncomfortable. Another drawback is presented by the impedance temporal dependence, caused by gel dehydration (Geddes and Valentinuzzi 1973). Spiked electrodes, on the other hand, can be used without any sort of skin preparation as the micromachined needles can go through the superficial layer of the SC significantly reducing the contact impedance. In figure 6, a 16-needle electrode simulation is shown. All needles are 40 μm in diameter, to match the electrodes presented by Griss *et al* (2002). The needles are symmetric and only penetrate the tissue for a very small

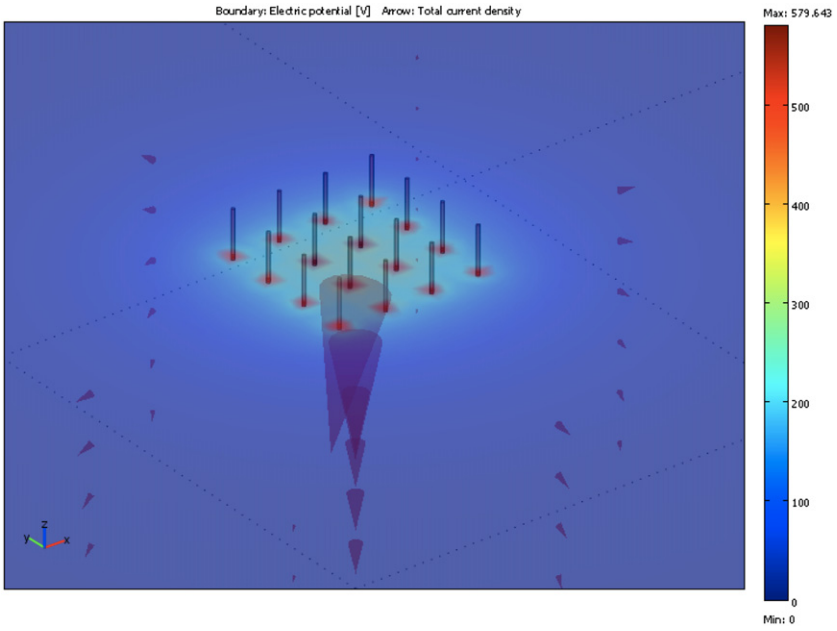

Figure 6. 16 spike-electrode.

part of their length. The current density is applied to the top face of the needles and results in a current vector arrow pointing downward within the tissue.

One of the key aspects that can be evaluated with the FEM simulator is contact impedance sensitivity to variations in the SC layer. The SC water content can be subject to variations causing a change in SC permittivity (ε) and conductivity (σ), as well as thickness (Sato *et al* 2000). A 10% decrease in both conductivity and permittivity and a 10 μm increase in its thickness have been simulated as case studies. These are reasonable changes and it must be noted that even larger variations could be expected, as the SC thickness can vary from tens to hundreds of μm in different body areas (McAdams *et al* 1996). We hypothesize that flat electrodes are influenced by such changes, while penetration of spiked electrodes offers a degree of immunity enabling it to be in direct contact with the underlying skin layer.

4. Results and discussion

4.1. Comparison between different simulation setups

The preliminary study with the 2D geometry (figure 2) shows that, whenever possible, a 2D simplification is highly advisable, as similar simulation results to the 3D setup (figure 3), with a much smaller computational cost, can be obtained. The difference in the evaluated impedance between the 2D ($|\mathbf{Z}| = 42\,092\ \Omega$) and 3D simulations ($|\mathbf{Z}| = 41\ 932\ \Omega$) is within 0.4%. It is also interesting to note that almost the entire potential drop is confined in the SC, as can be seen in figure 3. This was to be expected as the underlying skin volume is highly conductive and is in agreement with the simulations performed by Martinsen *et al* (1999), which shows that this is the case for frequencies up to 1 kHz.

The simplified one-electrode setup in figure 4 shows that the evaluated impedance is, as expected, slightly smaller than half of the previous one. In this case, only one electrode is considered, and the high-conductive volume is also reduced. When the volume under study

Table 1. Comparison between different simulation setups and measurements at 20 Hz.

		Re{Z} (Ω)	Im{Z} (Ω)	$\|Z\|$ (Ω)
Measured data	Two round electrodes (measured values) (Yamamoto and Yamamoto 1976)	30 000	5000	30 400
Simulated data	2D two-square electrodes (figure 2)	38 644	16 685	42 092
	3D two-square electrodes (figure 3)	38 498	16 619	41 932
	3D single-square electrode (figure 4)	17 609	8347	19 487
	3D single-square-electrode expanded geometry (figure 5)	15 880	7585	17 598

is enlarged in the x–y direction (to avoid fringing effects), the contact impedance is slightly reduced because of additional current flowing in this plane. Table 1 summarizes the results for these simulations.

In table 1, the simulated data have also been compared with the measurements presented by Yamamoto and Yamamoto (1976), where circular electrodes of a comparable size (diameter of 0.9 cm at a 5 cm distance) have been used along with a conductive gel. The gel impedance and additional effects due to electrode polarization and wire strays have been subtracted by the authors. This was done by measuring the direct electrode-to-electrode impedance, so the measured impedance is related to the SC and the underlying skin, as in the present work. The simulated data can be seen to be comparable with the measured data by Yamamoto and Yamamoto (1976). As can be seen, the impedance values are quite high for the flat electrodes. For this reason, such electrodes are more commonly used with the aid of a conductive gel, but in this work only dry electrodes are considered as a mean to study the impact of different electrode geometries. It must be noted that an extensive comparison with the literature could not be undertaken, as all the presented works systematically disagree on the reported impedance values (Geddes *et al* 1971, Yamamoto and Yamamoto 1976, McAdams *et al* 1996, Searle and Kirkup 2000, Chi *et al* 2010, Gandhi *et al* 2011).

4.2. Impact of the contact area on flat electrodes

The graph in figure 7 shows $|\mathbf{Z}|$ as a function of the electrode effective area for a 1 cm $\times$ 1 cm square electrode.

As expected, the effective area of contact is a key factor in the contact impedance. Measurements have shown that rough-surface electrodes can be used in order to optimize this parameter (McAdams *et al* 1996). A regression has been applied to the simulated data in order to obtain an analytical expression for $|\mathbf{Z}|$ as a function of frequency and area. The model fits well at low frequencies but does not provide accurate data when used at 2 kHz. This is not unexpected, as shown by Martinsen *et al* (1999); at 1 kHz the underlying skin starts dominating the impedance. This is why the analytical model, which predicts impedance for the stratum corneum, would give a negative value for the impedance at frequencies greater than 1 kHz, as shown in figure 7. The analytical expression is discussed in section 4.5.

4.3. Micromachined multipoint spiked electrodes

Table 2 summarizes the results of the simulated variations in the SC conductivity and thickness. As hypothesized in section 3.3, the flat electrodes exhibit a high sensitivity to such changes,

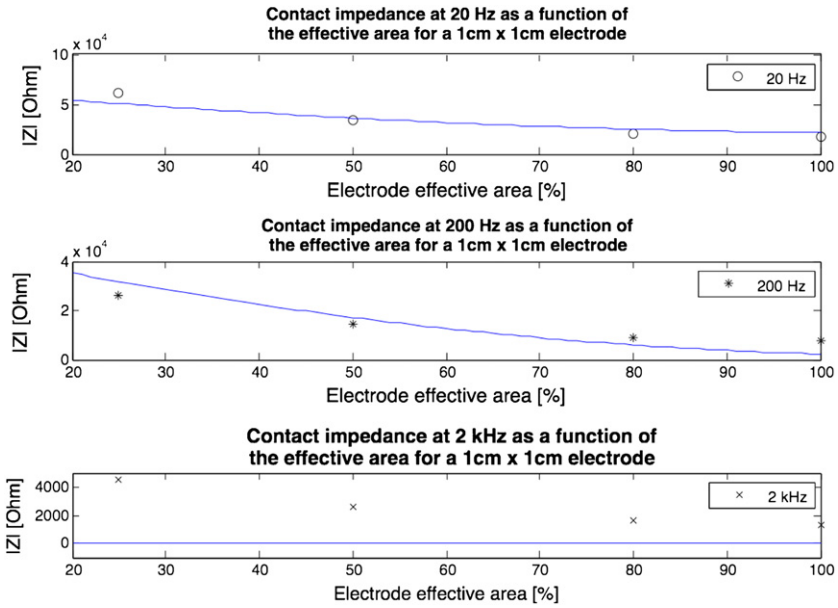

Figure 7. Contact impedance as a function of electrode effective area. The plotted data points are from the FEM simulation and the solid line the fitted regression model.

Table 2. Contact impedance sensitivity to stratum corneum changes.

	$\|Z\|$ (Ω) σ, ε nominal	$\|Z\|$ (Ω) σ, ε -10% thickness $+10$ μm	Δ (%)
Flat 20 Hz	17 598	25 594	45
16 needles 20 Hz	1155	1146	−0.8
Flat 200 Hz	7544	10 964	45
16 needles 200 Hz	1005	997	−0.8
Flat 2 kHz	1323	1910	44
16 needles 2 kHz	922	915	−0.8

while the spiked electrodes, thanks to their penetration depth set in this example to be 72 μm, are immune.

It is shown that if this value is constant, even a change in the SC conductivity, permittivity or thickness is negligible. Nevertheless, in a real-life scenario, the applied force is variable and will result in varying depth. Moreover, the number of needles in contact with the skin can decrease due to surface roundness or electrode damage. Figure 8 shows impedance variations for a 16-spike electrode due to penetration depth changes, while figure 9 shows contact impedance as a function of the number of spikes. Again, a regression has been applied to the simulated data in order to obtain an analytical model to predict the contact impedance and fits well with the data.

As shown in figures 8 and 9, the penetration depth and the number of spikes are crucial parameters and can result in significant impedance variability.

4.4. Limitations

Although it has been shown how a FEM EM simulator can provide enough flexibility to study different geometries and directly allow for the evaluation of impedance values, it must be

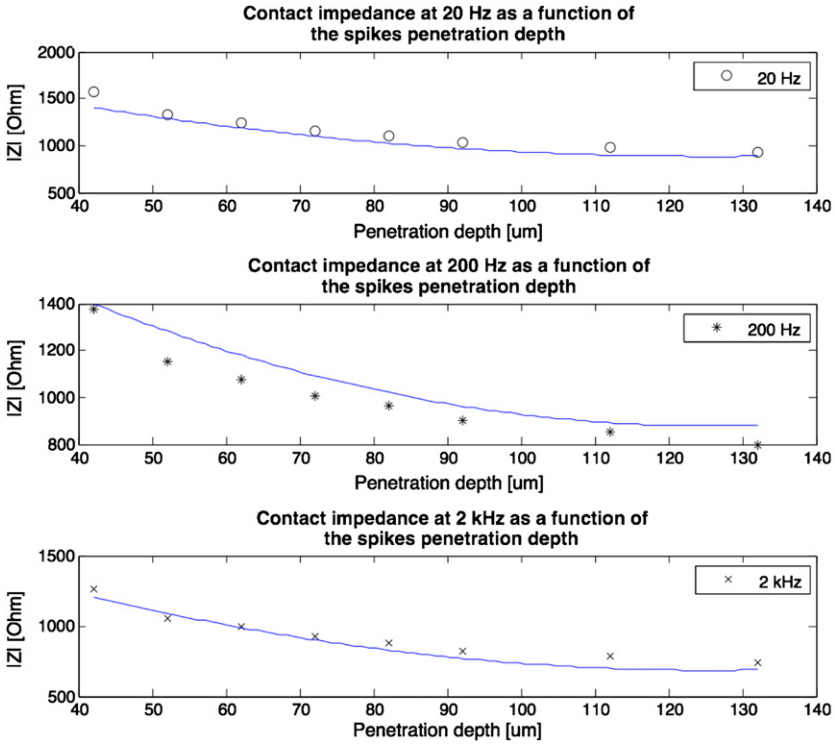

Figure 8. Contact impedance as a function of the penetration depth. The plotted data points are from the FEM simulation and the solid line the fitted regression model.

noted that there are several limitations to this method. The presented results outline how, even when the same electrodes are used, great variability in the contact impedance can occur due to setup mismatches such as the area of contact for flat electrodes or the penetration depth for spiked electrodes.

Nevertheless there are other effects that cannot be simulated in such environment. The major limitation is due to the electrochemical nature of the electrodes. An electrode constitutes the site of a charge carrier shift, a charge exchange between electrons and ions (Grimnes 1983). At this interface, electrochemical processes occur, with effects such as half-cell potentials and electrical double layer, causing additional dc voltages and series capacitors and resistors.

Moreover, the underlying skin becomes moistened with time due to sweat-gland activity, thereby decreasing the electrode–skin impedance (Geddes and Valentinuzzi 1973).

4.5. Analytical model for the electrode–skin interface

As shown in figures 7–9, an analytical formula provides a reasonable approximation of the contact impedance. This allows one to quickly estimate the impedance for flat or spiked electrodes as a function of the area, the number of spikes and their penetration depth. Table 3 shows the analytical formula for the different scenarios where f, A, s and d represent the frequency, area, number of spikes and penetration depth, respectively. The coefficient of determination $\mathbf{R^2}$ is evaluated in order to provide a measure of quality for the statistical regression. The analytical formula is obtained with a regression algorithm and is truncated

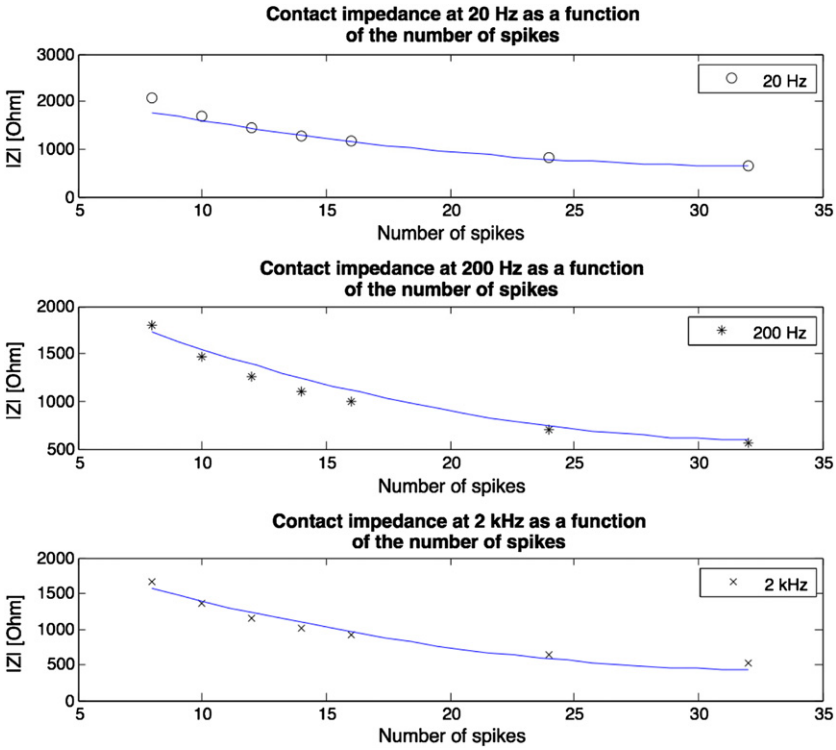

Figure 9. Contact impedance as a function of the number of spikes. The plotted data points are from the FEM simulation and the solid line the fitted regression model.

Table 3. Analytical model for the electrode–skin interface.

	$\|Z\|$	R^2
Flat electrode, $\|Z\| = \max(0, \|Z\|(f, A))$	$\|Z\| = 7.1 \times 10^4 - 8.7 \times 10^8 A - 5.3 \times 10 f + 3.8 \times 10^{12} A^2$	0.93
Spiked electrode, $\|Z\|(f, s)$	$\|Z\| = 2.6 \times 10^3 - 1.2 \times 10^2 s - 2.8 \times 10^{-1} f + 1.8 s^2$	0.95
Spiked electrode, $\|Z\|(f, d)$	$\|Z\| = 1.5 \times 10^3 - 1.4 \times 10 d - 2.0 \times 10^{-2} f + 7.4 \times 10^{-2} d^2$	0.87

at the second order as higher order expressions failed to further improve the coefficient of determination $\mathbf{R^2}$. This is defined as

$$\mathbf{R}^2 = 1 - \frac{\mathrm{SS}_{\mathrm{err}}}{\mathrm{SS}_{\mathrm{tot}}}, \tag{9}$$

where $\mathrm{SS}_{\mathrm{tot}}$ and $\mathrm{SS}_{\mathrm{err}}$ are defined respectively as

$$\mathrm{SS}_{\mathrm{tot}} = \sum_i (y_i - \mu)^2 \tag{10}$$

$$\mathrm{SS}_{\mathrm{err}} = \sum_i (y_i - f_i)^2, \tag{11}$$

with y_i and f_i being the simulated and predicted values, respectively, and μ the mean of the simulated data.

Although the analytical expression, as seen in section 4.2, gives zero impedance values for flat electrodes at high frequencies, the evaluated $\mathbf{R^2}$ value is still high in this case. This

is explained by the fact that the impedance at these frequencies is much smaller than at lower frequencies and therefore has a smaller impact on the coefficient of determination. The presented expressions are intended to give a rough estimate of the impedance variations for a 16-spike electrode. Therefore, two separate expressions are given: one as a function of frequency and penetration depth, the other as a function of frequency and number of spikes. Penetration depth is not directly measurable; therefore, the user should only use such expressions to estimate variability ranges.

5. Conclusions

In this work, flat and micromachined multipoint spiked electrodes have been simulated in order to investigate their sensitivity to geometrical parameters and variability in skin properties. It has been shown how flat electrodes are more susceptible to variations when the most superficial layer of skin is not constant, while spiked electrodes, due to their ability to go through this layer, are immune to such changes. Flat electrodes are also influenced by the mechanical setup that can reduce the contact area, but the same is true for micromachined multipoint spiked electrodes as different pressures can result in different penetration depths and hence different contact impedances. Although FEM EM simulations explain the relationship between electrode geometries and contact impedance, biological effects cannot be modeled and thus it is crucial to explore new ways to measure contact impedance while performing clinical EEG and EIT. Finally, analytical expressions are given as a way to quickly estimate the contact impedance. These were more successful at fitting the spiked electrodes than the flat electrodes, which are influenced by the capacitive nature of the stratum corneum.

References

Boone K G and Holder D S 1996 Effect of skin impedance on image quality and variability in electrical impedance tomography: a model study *Med. Biol. Eng. Comput.* **34** 351–4

Bowtell R and Bowley R 2000 Analytic calculations of the E-fields induced by time-varying magnetic fields generated by cylindrical gradient coils *Magn. Reson. Med.* **44** 782–90

Boyle A and Adler A 2011 The impact of electrode area, contact impedance and boundary shape on EIT images *Physiol. Meas.* **32** 745–54

Brown B H 2003 Electrical impedance tomography (EIT) a review *J. Med. Eng. Technol.* **27** 97–108

Chi Y M, Jung T-P and Cauwenberghs G 2010 Dry-contact and noncontact biopotential electrodes: methodological review *IEEE Rev. Biomed. Eng.* **3** 106–19

Comsol Multyphysics 2011 www.comsol.com

Degen T and Jackel H 2008 Continuous monitoring of electrode–skin impedance mismatch during bioelectric recordings *IEEE Trans. Biomed. Eng.* **55** 1711–5

Gabriel C, Gabriel S and Corthout E 1996 The dielectric properties of biological tissues: I. Literature survey *Phys. Med. Biol.* **41** 2231–49

Gandhi N, Khe C, Chung D, Chi Y M and Cauwenberghs G 2011 Properties of dry and non-contact electrodes for wearable physiological sensors *Int. Conf. on Body Sensor Networks (BSN) (23–25 May 2011)* pp 107–12

Geddes L, Da Costa C and Wise G 1971 The impedance of stainless-steel electrodes *Med. Biol. Eng. Comput.* **9** 511–21

Geddes L and Valentinuzzi M 1973 Temporal changes in electrode impedance while recording the electrocardiogram with 'Dry' electrodes *Ann. Biomed. Eng.* **1** 356–67

Gonçalves S, de Munck J C, Heethaar R M, Lopes da Silva F H and van Dijk B W 2000 The application of electrical impedance tomography to reduce systematic errors in the EEG inverse problem—a simulation study *Physiol. Meas.* **21** 379–93

Gramatica F, Carabalona R, Casella M, Cepek C, Di Fabrizio E, Di Rienzo M, Gavioli L, Matteucci M, Rizzo F and Sancrotti M 2006 Micropatterned non-invasive dry electrodes for brain–computer interface *3rd IEEE/EMBS Int. Summer School on Medical Devices and Biosensors (4–6 September 2006)* pp 69–72

Grimnes S 1983 Impedance measurement of individual skin surface electrodes *Med. Biol. Eng. Comput.* **21** 750–55

Griss P, Tolvanen-Laakso H K, Merilainen P and Stemme G 2002 Characterization of micromachined spiked biopotential electrodes *IEEE Trans. Biomed. Eng.* **49** 597–604

Guermandi M, Cardu R, Franchi E and Guerrieri R 2011 Active electrode IC combining EEG, electrical impedance tomography, continuous contact impedance measurement and power supply on a single wire *IEEE Solid-State Circuits (ESSCIRC), European Conf. (September 2011)* pp 335–38

Holder D 2004 *Electrical Impedance Tomography: Methods, History, and Applications* (Beograd: Institute of Physics)

Hua P, Woo E J, Webster J G and Tompkins W J 1993 Finite element modeling of electrode–skin contact impedance in electrical impedance tomography *IEEE Trans. Biomed. Eng.* **40** 335–43

Huhta J C and Webster J G 1973 60 Hz interference in electrocardiography *IEEE Trans. Biomed. Eng.* **20** 91–101

Martinsen Ø G, Grimnes S and Haug E 1999 Measuring depth depends on frequency in electrical skin impedance measurements *Skin Res. Technol.* **5** 179–81

McAdams E, Jossinet J, Lackermeier A and Risacher F 1996 Factors affecting electrode–gel–skin interface impedance in electrical impedance tomography *Med. Biol. Eng. Comput.* **34** 397–408

McEwan A, Cusick G and Holder D S 2007 A review of errors in multi-frequency EIT instrumentation *Physiol. Meas.* **28** S197–215

Michel C M, Murray M M, Lantz G, Gonzalez S, Spinelli L and de Peralta R G 2004 EEG source imaging *Clin. Neurophysiol.* **115** 2195–222

Rabaey J M 2011 Brain–machine interfaces as the new frontier in extreme miniaturization *Proc. European Conf. on Solid-State Device Research (ESSDERC) (12–16 September 2011)* pp 19–24

Sato J, Yanai M, Hirao T and Dendaet M 2000 Water content and thickness of the stratum corneum contribute to skin surface morphology *Arch. Dermatol. Res.* **292** 412–7

Searle A and Kirkup L 2000 A direct comparison of wet, dry and insulating bioelectric recording electrodes *Physiol. Meas.* **21** 271–83

Spinelli E M, Mayosky M A and Pallas-Areny R 2006 A practical approach to electrode–skin impedance unbalance measurement *IEEE Trans. Biomed. Eng.* **53** 1451–3

Tri J-L, Severson R P, Firl A R, Hayes D L and Abenstein J P 2005 Cellular telephone interference with medical equipment *Mayo Clin. Proc* **80** 1286–90

Wang W and Eisenberg S R 1994 A three-dimensional finite element method for computing magnetically induced currents in tissues *IEEE Trans. Magn.* **30** 5015–23

Winter B B and Webster J G 1983 Driven-right-leg circuit design *IEEE Trans. Biomed. Eng.* **30** 62–6

Wise K D, Anderson D J, Hetke J F and Kipke D R 2004 Wireless implantable microsystems: high-density electronic interfaces to the nervous system *Proc. IEEE* **92** 76–97

Yamamoto T and Yamamoto Y 1976 Electrical properties of the epidermal stratum corneum *Med. Biol. Eng. Comput.* **14** 151–8

Yamamoto T and Yamamoto Y 1986 Characteristics of skin admittance for dry electrodes and the measurement of skin moisturisation *Med. Biol. Eng. Comput.* **24** 71–7